RE-DISTRIBUTION OF ANTIBIOTIC WITHIN A COMMUNITY IS BEHIND THE UNPREDICTABLE CHANGE IN EFFICACY OBSERVED IN CLASSIC LABORATORY ASSAYS

CARLOS REDING[1,2]

[1] *Department of Biosciences, University of Exeter, EX4 4QD, United Kingdom.*

[2] *Department of Genetics, School of Medicine, Stanford University. Stanford, CA 94304.*

***Corresponding author:** `rc_reding@teknik.io`

Microbes live in complex communities that are often difficult to study. Thus, whether they alter the response to environmental stressors in its member species is not still well understood. Here I show that community members change the distribution of antimicrobial molecules among their member species depending on their drug sensitivity. This re-distribution of drug changes the efficacy of antimicrobials with respect to laboratory assays that use pure cultures. Importantly, the resulting drug efficacy can be qualitatively predicted and therefore estimate whether a specific neighbour will increase or decreased drug efficacy against a focal species. The efficacy of tetracycline against *Escherichia coli* MC4100 changed consistently with my theoretical predictions when grown alongside a drug sensitive and non-sensitive neighbours, resulting in the loss or boost of tetracycline efficacy. My study suggests a physical mechanism to explains this phenomenon, often considered unpredictable, highlighting the potential of synthetic neighbours to curb drug sensitivity.

I. Introduction

The notion of 'pure culture', where a genotype is isolated and grown in purified form, is fundamental in microbiology. Their use is imposed by the unreliability of *in vitro* assays when cultures contain multiple species (*1*, *2*). But here is the problem: Microbes live in nature as part of wider communities (*3*). The use of antimicrobials and how they lead to resistance is particularly sensitive to this problem. Therapy design and evolutionary studies rely on pure cultures to measure drug sensitivity (*4*) and speed of evolution (*5*) to estimate optimal conditions for selection of resistance. Perhaps not surprisingly, given the formation of communities in the microbial world, antimicrobial therapies often fail with polymicrobial infections (*6*). Indeed, recent evidence suggests (*7–9*) that antimicrobial efficacy may depend on surrounding species. But, why?.

Below I present a model that provides a physical mechanism to explain and predict this phenomenon. Reliance on common resources can suppress the growth of competing species, whence the concept of *competitive suppression* (*10*). The model suggests that carbon and antimicrobial molecules spread across all species within a community. Competitive suppression may limit the growth of all species within the community, but if the drug sensitivity of the member species is comparable, the antimicrobial diffuses into all species—not just the target—resulting in fewer antimicrobial molecules per species. That is, loss of drug efficacy. Phenotypically, this can be interpreted as drug tolerance of the individual species, but it is not: It is under-exposure, driven

by the withrawal of antimicrobial molecules by neighbouring species. However, if some species are *not* as sensitive to the drug, competitive suppression enforces the uneven distribution of antimicrobial. The result a rise in drug molecules per cell in the most sensitive species, and improved drug efficacy. To validate these predictions I used two sets of pairwise competition assays between two constructs of *Escherichia coli*, sensitive and resistant to the antibiotic tetracycline, and *Salmonella typhimurium*, also sensitive to the drug.

II. Results

Drug response of a focal species is determined by susceptibility of its neighbouring species. Consider j phenotypically distinct species competing for a limited resource, C, and exposed to a drug, A, supplied at concentration $A_e(0) = A_0$, cast as the following model:

$$\dot{S}_j = \overbrace{G_j(C)S_j}^{\text{Growth}} \cdot \overbrace{I_j(A)}^{\text{Inhibition}}, \tag{1a}$$

$$\dot{A}_j = \overbrace{-dA_j}^{\text{Decay}} + \overbrace{\varphi_j(A_e - A_j)S_j}^{\text{Fick's Diffusion}}, \tag{1b}$$

$$\dot{A}_e = -dA_e - \sum_{j=1}^{i} \varphi_j(A_e - A_j)S_j, \tag{1c}$$

$$\dot{C} = -\sum_{j=1}^{i} \overbrace{U_j(C)S_j}^{\text{C-Uptake}}, \tag{1d}$$

Here, $\dot{S}_j$ and $\dot{A}_j$ represent the density of individuals per unit volume from species j and their content of drug A over time, respectively, with initial conditions $S_j(0) = S_{j0}$ and $A_j(0) = 0$. $U_j(C)$, the uptake rate of resource C—supplied at concentration C_0—of individuals from species j, is a saturating Monod function proportional to the maximal uptake rate,

$$U_j(C) := \bar{\mu}_j \frac{C}{K_j + C}, \tag{2}$$

where K_j is the half-saturation parameter and the affinity of individuals from species j for the limited resource C is given by $1/K_j$. Their growth rate (i.e. absolute fitness) at a given resource concentration is denoted by $G_j(C) := U_j(C) \cdot y_j$, where y_j is the biomass yield per unit of resource in individuals from species j. Their growth inhibition, by drug A, is described qualitatively by the inhibition function (*11*)

$$I_j(A) := \frac{1}{1 + (A_j/\kappa_j)^\alpha}, \text{ where } 0 \leq I_j(A) \leq 1. \tag{3}$$

This function is dimensionless and has two parameters. First, the Hill coefficient α which characterises the co-operativity of the inhibition. And second, κ_j is the affinity of drug A for its target and it can be derived from the drug concentration required to halve the maximal growth rate, so that $A_{50} = 1/\kappa_j$ (*11*). For the sake of simplicity, I assumed that drug A diffuses from the environment into cells of species j, and *vice versa*, with a diffusion coefficient φ_j; and part

of A being lost to chemical stability (12) at a rate d. Indeed, antimicrobials can diffuse through cell membranes facilitated by membrane proteins (13), but they can also actively up-taken by transporters (13).

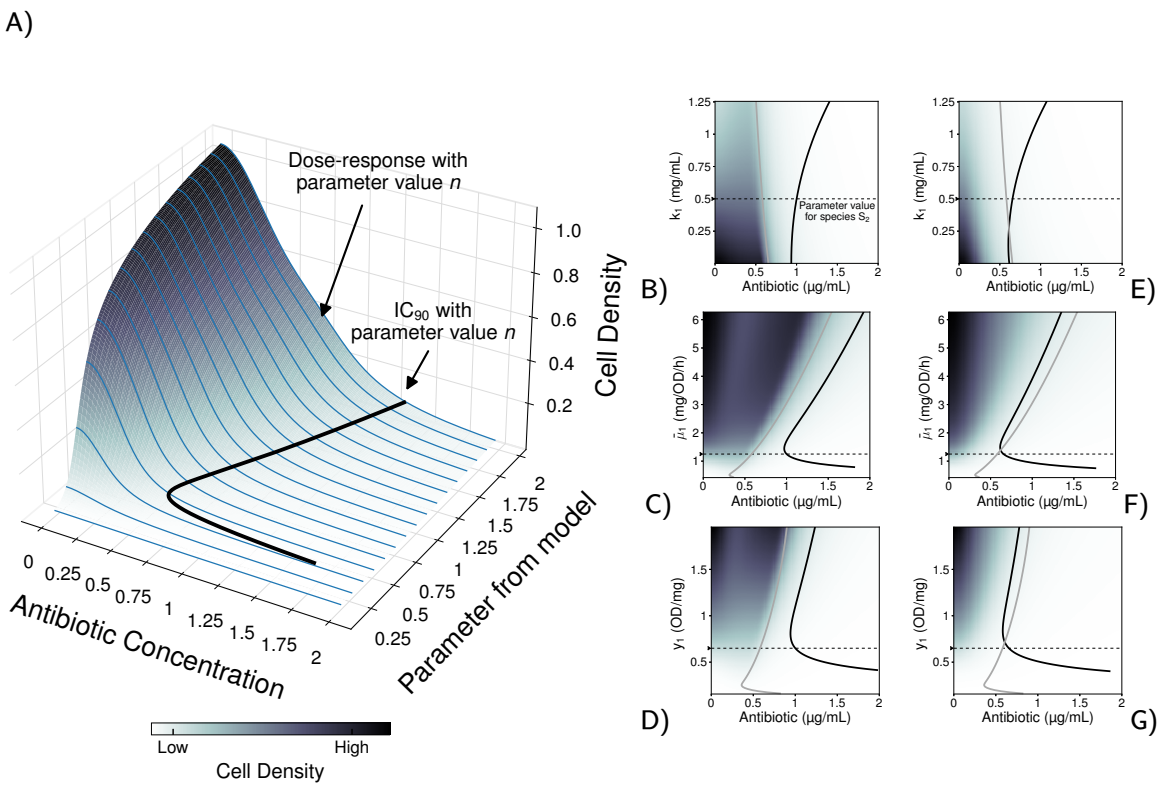

Figure 1. S_1 drug sensitivity profiles in pure and mixed culture growth conditions alongside species S_2. A) Growth of species S_1, with different parameter values ($k_1, \bar{\mu}_1$, and y_1), after 24h of growth in the presence of different antibiotic concentrations. I aggregated the resulting dose-response profiles (blue) to create a density map from low predicted cell density (white) to high predicted cell density (black). **B–D)** IC_{90}, antibiotic concentration inhibiting 90% (IC_{90}) the growth predicted without drug, resulting with different parameters values for the half-saturation parameter k_1 (B), maximal carbon up-take $\bar{\mu}_1$ (C), or biomass yield y_s (D) in equation 1 when species S_2 is drug-sensitive. The IC_{90} for species S_1 growing as pure cultures is shown in grey, and growing in mixed culture with S_2 are shown in black. The parameter values for species S_2 were fixed at a value noted by a black arrow on the y-axis, followed by a dotted black line. **E–G)** Change in IC_{90}, as in Figures B–C), when the competing species S_2 is *not* drug-sensitive (resistant or tolerant).

For my first computation I set the number of species $j = 2$, to facilitate later experimental validation, where $I_1(A) = I_2(A)$ and $G_1(C) = G_2(C)$. Thus, individuals from both species are sensitive to A and phenotypically identical. Given Equation 3, the density of individuals from either species as pure cultures, after 24h of incubation, declines with higher drug concentrations consistently with standard clinical protocols (4) (Figure 1A). To allow experimental validation, I calculated the concentration of A inhibiting the growth of the pure cultures by 90% (IC_{90}) as commonly used in clinic laboratories (14–16). The drug sensitivity of each species depends on the values for the parameters $K, \bar{\mu}$, and y of Equation 2 (Figure 1B–D, grey), with values that increase the density of individuals resulting in higher IC_{90}. This is consistent with the *inoculum effect* (17), whereby sensitivity tests that use larger inocula also report higher minimum inhibitory concentrations, hence the standardisation of these clinical assays. However, the

relationship between these parameters and the IC_{90} is not necessarily proportional. For parameters $\bar{\mu}$ and y, for example, the resulting mange in IC_{90} with respect to the parameter values is non-monotone, which means certain values for these parameters can maximise susceptibility for drug A. The neighbouring species shows similar, albeit not identical, changes in sensitivity (Figure S2).

This phenomenon is exacerbated if both species grow in mixed culture conditions, where both become phenotypically more tolerant to drug A (Figure 1B–D, black). If I were to target, say, individuals from species S_1, doing so when the species is surrounded by S_2 would require more drug. This is the case, for example, of pancreatic ductal adenocarcinoma treated with gemcitabine when bacteria grow within the tumour's microenvironment (*18*). More generally, genotypes analog to S_1 should increase their drug tolerance when they are surrounded by similarly sensitive species.

To test this hypothesis, I mixed equal proportions (cell/cell) of *Escherichia coli* Wyl and *Salmonella typhimurium* SL1344 in minimal media supplemented with different concentrations of tetracycline (see Methods). This antibiotic can diffuse passively into cells of both gram-negative species (*19*), who also have similar sensitivity to this antibiotic. 0.232 ± 0.003 and 0.276 ± 0.016 µg/mL of tetracycline (mean $IC_{90} \pm 95\%$ confidence, with $n = 8$ replicates, see Methods). This approximates to $I_1(A) \approx I_2(A)$, as laid out by the theory above. The chromosome of *E. coli* Wyl carries *yfp*, gene encoding a yellow fluorescence protein (YFP), so I tracked its density in mixed culture conditions. Consistently with Equations 1a–d, the bacterium was around 23% more tolerant to tetracycline when it grew in mixed culture with *S. typhimurium* (Mann-Whitney U-test $p = 1.554 \times 10^{-4}, ranksum = 36$ with $n = 8$ replicates, Figure 2A).

Next, I explored in the model the case where individuals from both species have different sensitivities to drug A ($I_1(A) \neq I_2(A)$). This scenario is akin to pathogens such as *C. difficile* growing alongside human cells (*20*) where the latter are unaffected by the drug ($I_2(A) \approx 1$). The model now predicts a subset of values for K, y, and $\bar{\mu}$ that make S_1 *more* sensitive to the drug in the presence of individuals from species S_2 (Figure 1E–G). The neighbour species, being less susceptible to the drug, shows little change in sensitivity (Figure **??**). The prediction is similar to that where the neighbour species is resistant to A through efflux pumps (*21*) (see Supplementary Text). To test this prediction, I mixed equal proportions (cell/cell) of two constructs of *Escherichia coli* with different sensitivities to tetracycline. One construct is Wyl, used above, who is sensitive to the antibiotic. The other construct is GB(c), harbouring a non-transmissible plasmid carrying the gene *tet(36)* (*22*) and, therefore, resistant to the drug. Tetracycline binds to the bacterial ribosome, inhibiting protein synthesis (*23*), and *tet(36)* provides ribosomal protection against tetracycline (*22*) without degrading the antibiotic. The IC_{90} for this construct was 6.106 ± 0.272 µg/mL of tetracycline (mean $IC_{90} \pm 95\%$ confidence with $n = 8$ replicates). Now, $I_1(A) \ll I_2(A)$ satisfies the assumption above. The IC_{90} for *E. coli* Wyl was 0.232 ± 0.003 µg/mL of tetracycline as pure culture. Growing alongside drug-resistant GB(c), however, it was 0.112 ± 0.003 µg/mL (Figure 2B).

Drug uptake by species S_2 determines drug availability for S_1. Above I noted that parameter values leading to higher density of individuals in pure culture, also led to higher

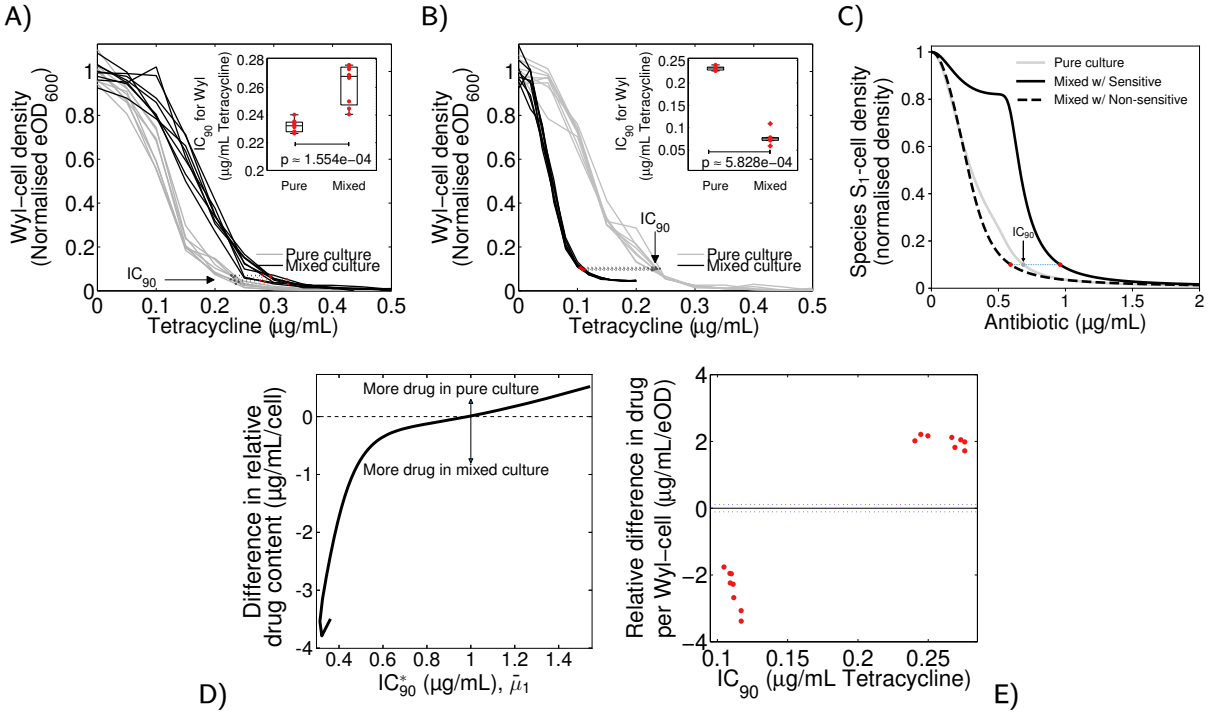

Figure 2. Change in drug efficacy against sensitive *Escherichia coli* Wyl are consistent with theoretical predictions. A–B) Change in normalised density of *Escherichia coli* Wyl as a function of tetracycline concentration, when Wyl grows in mixed culture with tetracycline-sensitive *Salmonella typhimurium* (A) and tetracycline-resistant *Escherichia coli* GB(c) (B). The change in density of Wyl growing in mixed culture is shown in black, with grey showing the change in density in pure culture. The IC_{90} in each condition is shown as dots, red for mixed culture conditions and dark grey for pure culture, connected by a dotted line. Non-parametric, Mann-Whitney U-test between IC_{90}s is shown in the inset. Raw data is shown as dots, whereas the boxes represent median (centre of the box), 25th, and 75th percentile of the dataset. The whiskers show the most extreme data points that are not outliers. **C)** Theoretical change in S_1-cell density with increasing antibiotic concentration in pure (grey) and mixed (black) culture conditions with neighbours that have different drug sensitivity. The plot represents the case where both species have different carbon uptake (μ_i), and differences in IC_{90} are represented as shown in A–B for consistency. **D)** Difference in drug content per S_1-cell at the IC_{90} between pure culture and mixed culture conditions. Positive and negative values denote more drug in S_1-cells in pure and mixed culture conditions, respectively. Lack of difference is shown as a horizontal, dotted line. **E)** Experimental estimation of the difference in relative cell content in the bacterium *Escherichia coli* Wyl. Raw data for Wyl is shown as red dots. Lack of difference is shown as a horizontal, black line and the 95% confidence of the lack of difference as a horizontal, dotted line. Insets in A and B, and raw data for relative drug content can be found in Figure S3.

IC_{90}. When $I_1(A) \approx I_2(A)$, Equations 1a–d suggest that individuals from one species change the drug availability, measured as relative drug molecules per individual, for the other. Thus, when species S_2 captures through diffusion its share of drug in mixed culture conditions, there is less of it available for species S_1 resulting in less drug per individual (Figure S1A–C)—and *vice versa*. However, when $I_1(A) \neq I_2(A)$, by virtue of different affinities of drug A for each species ($\kappa_1 \neq \kappa_2$), the drug diffuses more rapidly from the least sensitive species back into the environment—re-exposing its sensitive counterpart. Thus, the change in drug content in the most sensitive species occurs through a different mechanism. The least sensitive species, given its higher tolerance to antimicrobial A, can maintain its growth and therefore it can remove a higher

share of the limited resource, C. Consequently, the growth of the most sensitive species is limited (*10*), leaving more drug per individual of this species (Figure S1D–F). This competition for a shared resource is akin to that found, for example, between *Salmonella typhimurium* biofilms and cancer cells, where they compete for access to nutrients in the bloodstream—resulting in the bacteria inhibiting cancer growth (*24*).

To verify this hypothesis, I estimated the content of tetracycline in *E. coli* Wyl by dividing the bacterium's culture density, measured in relative fluorescence units to allow tracking in mixed culture conditions, by the concentration of tetracycline defining its IC_{90}. The estimates resemble closely the theoretical predictions in Figure 2C: *E. coli* Wyl contains approximately 20% less tetracycline growing next to *Salmonella typhimurium* (Figure 2D) and 65% more tetracycline growing alongside drug-resistant GB(c) (Figures 2E).

III. Discussion

All models are wrong, but some are useful. Standard microbiological assays from clinical microbiology (*1*, *2*) to evolutionary biology (*25*) rely on pure cultures to measure drug sensitivity, study evolutionary processes, and more. But these assays miss the interactions that microbes engage with its neighbours in nature, and how these interactions may change the traits analysed. Microbial communities are complex and, unfortunately, there are experimental limitations that hinder the study of these communities—like the number of fluorescent proteins that can be used simultaneously without spectral overlap (*26*).

The mathematical model that I present to study this complexity is, like all models, wrong in some ways. But it is also useful in others. The limitations of the model are imposed by some experimental conditions. For example, for simplicity the Fick's term has no spacial derivative as it would be expected, as I shaked the culture to maintain the growth conditions homogeneous (see Methods). Instead, the derivative is approximated as the difference in antimicrobial inside and outside the cells. Another assumption from the model is that all j species rely upon a single source of carbon. In reality, however, I used two: Glucose, the main carbon source, and casamino acids. The latter is added to provide the microbes with amino acids they cannot synthetise, and that they need to grow. But, true to the underlying microbial complexity, casamino acids can also be used as carbon source if glucose is scarce (*27*). Is this difference relevant? In this case I argue it is not. The goal of the study is to explore whether the number of cells from a competing species can change antibiotic efficacy against a focal species, and if they do, to understand why. Indeed, the use of two carbon sources may lead to, for example, speciation: Each species would evolve to utilise different carbon sources to avoid competition (*28*). This can also occur through byproducts of a single carbon source (*29*). But mine is not an evolutionary study.

The use of pure cultures in clinical and evolutionary assays is imposed by the unpredictability of drug efficacy, or adaptation to novel environments, when samples have mixed species (*1*, *2*). The contribution of my model is to show that, quite the opposite, the change in drug efficacy resulting from inter-species interactions responds to a specific mechanism and, thus, can be predicted. This theory can aid antimicrobial dose escalation or de-escalation if the sensitivity of all species exposed is known, helping to maximise drug efficacy. The two-fold increase in tetracycline efficacy that I reported here, however, highlights the potential that

synthetic neighbours may have to curb antimicrobial efficacy—reducing the amount of drug used, and therefore selection on resistance.

IV. Methods

Media and Strains. The strains of *Escherichia coli* GB(c) and Wyl were a gift from Remy Chait and Roy Kishony, and non-labelled *Salmonella typhimurium* SL1344 a gift from Markus Arnoldini and Martin Ackermann. Experiments were conducted in M9 minimal media supplemented with 0.4% glucose (Fisher Scientific #G/0500/53) and 0.1% casamino acids (Duchefa #C1301.0250), supplemented with tetracycline. M9 minimum media (50X) was made by mixing equal proportions (vol/vol) of two parts, part A and part B, and diluted accordingly to 1X. Part A (50X) contains 350 g/L of K_2HPO_4 (Sigma #P3786) and 100g/L of KH_2HPO_4 (Sigma #P9791); whereas part B (50X) contains 29.4g/L of trisodium citrate (Sigma #S1804), 50g/L of $(NH_4)_2SO_4$ (Sigma #A4418), and 10.45g/L of $MgSO_4$ (Fisher Scientific #M/1050/53). I made tetracycline stock solutions from powder stock (Duchefa #0150.0025) at 5mg/mL in deionised water. Subsequent dilutions were made from this stock and kept at 4^oC.

Sensitivity assay. I inoculated a 96-well microtitre plate, containing 150µL of media supplemented with 0–0.5 µg/mL of tetracycline (for *E. coli* Wyl and *S. typhimurium*) or 0–15µg/mL (for *E. coli* GB(c)), with an overnight of each strain to measure drug sensitivity in pure cultures. For sensitivity assays of Wyl in mixed culture conditions I inoculated the microtitre plate, containing 150µg/mL of media supplemented with 0–0.5 µg/mL of tetracycline, with equal number of cells from two overnight cultures from Wyl and *S. typhimurium* using 8 technical replicates for each drug concentration. For the competition between Wyl and GB(c), however, I used 0–0.2 g/mL to measure drug efficacy more reliably given the increased drug efficacy observed against Wyl.

I incubated the microtitre plate at 30^oC in a commercial spectrophotometer, shaking at 750rpm to ensure uniform mixing, and measured the optical density of each well at 600nm (OD_{600}), yellow florescence for Wyl (YFP excitation at 505nm, emission at 540nm), and cyan fluorescence for GB(c) (CFP at 430nm/480nm) every 20min for 24h. I defined the minimum inhibitory concentration as the tetracycline concentration able to inhibit 90% of the growth observed in the absence of antibiotic after the 24h incubation period.

Culture readings. Fluorescence protein genes were constitutively expressed with an approximately constant fluorescence to optical density ratio (Figure S4). The number of colony forming units (CFU) is positively correlated with optical density measured at 600nm (OD_{600}) (Figure S5). Thus, I normalised fluorescence readings with respect to optical density readings, using the ratio optical density to fluorescence that I in pure culture conditions, to track the relative abundance of Wyl in mixed culture conditions. This metric is referred to as 'Estimated optical density' in the main text. Time series data set were blank corrected prior to calculating the minimum inhibitory concentration.

Code availability: A non-parameterized, python3 implementation of equations 1a–d can be found at https://github.com/rc-reding/papers/tree/master/EvolProof_2020. Table 1 contains a list of parameter values used.

Table 1. Model parameters for Equations 1a–d, 2 and 3.

Parameter	Description	Value
$\bar{\mu}_j$	Maximal carbon uptake rate	1.25 mg / OD / h
K_j	Half-saturation constant	0.5 mg / mL
y_j	Biomass yield	0.65 OD / mg
d	Drug degradation rate	10^{-4} / h
κ_j	Affinity of drug A for species type j	0.1 mL / µg
φ_j	Diffusion coefficient	0.1 mL / OD / h
A_0	Initial drug concentration	2 µg / mL
C_0	Initial carbon concentration	2 mg / mL

Acknowledgements: The author thanks Robert Beardmore from the University of Exeter for laboratory support in the early stages of this study.

Competing interests: The author declares no competing interests.

References

1. Shahidi, A. & Ellner, P. D. Effect of mixed cultures on antibiotic susceptibility testing. *Appl. Microbiol.* **18,** 766–770 (1969).
2. Ellner, P. D. & Johnson, E. Unreliability of Direct Antibiotic Susceptibility Testing on Wound Exudates. *Antimicrob. Agents. Chemother.* **9,** 355–356 (1976).
3. Ghoul, M. & Mitri, S. The ecology and evolution of microbial competition. *Trends Microbiol.* **24,** 833–845 (2016).
4. *Performance Standards for Antimicrobial Susceptibility Testing; Twenty–Second Informational Supplement M100–S22* 3. Clinical and Laboratory Standards Institute (2012). ISBN: 1-56238-786-3.
5. Reding, C., Catalán, P., Jansen, G., *et al.* The Antibiotic Dosage of Fastest Resistance Evolution: gene amplifications underpinning the inverted-U. *Mol. Biol. Evol.* msab025. ISSN: 0737-4038 (Mar. 2021).
6. Simón-Soro, A. & Mira, A. Solving the etiology of dental caries. *Trends Microbiol.* **23,** 76–82 (2015).
7. Peters, B. M., Jabra-Rizk, M. A., Graeme, A., Costerton, J. W. & Shirtliff, M. E. Polymicrobial interactions: impact on pathogenesis and human disease. *Clin. Microbiol. Rev.* **25,** 193–213 (2012).
8. Lasa, I. & Solano, C. Polymicrobial infections: Do bacteria behave differently depending on their neighbours? *Virulence* **9,** 895–897 (2018).

9. Galera-Laporta, L. & Garcia-Ojalvo, J. Antithetic population response to antibiotics in a polybacterial community. *Sci. Adv.* **6,** eaaz5108 (2020).

10. Day, T., Huijben, S. & Read, A. F. Is selection relevant in the evolutionary emergence of drug resistance? *Trends Microbiol.* **23,** 126–133 (2015).

11. Klumpp, S., Zhang, Z. & Hwa, T. Growth rate-dependent global effects on gene expression in bacteria. *Cell* **139,** 1366–1375 (2009).

12. Gómez-Pacheco, C., Sánchez-Polo, M, Rivera-Utrilla, J & López-Peñalver, J. Tetracycline degradation in aqueous phase by ultraviolet radiation. *Chem. Eng. J.* **187,** 89–95 (2012).

13. Braun, V., Bös, C., Braun, M. & Killmann, H. Outer membrane channels and active transporters for the uptake of antibiotics. *The J. Infect. Dis.* **183,** S12–S16 (2001).

14. Cedillo-Rivera, R & Munoz, O. In-vitro susceptibility of Giardia lamblia to albendazole, mebendazole and other chemotherapeutic agents. *J. Med. Microbiol.* **37,** 221–224 (1992).

15. Cottrell, M. L., Hadzic, T. & Kashuba, A. D. Clinical pharmacokinetic, pharmacodynamic and drug-interaction profile of the integrase inhibitor dolutegravir. *Clin. Pharmacokinet.* **52,** 981–994 (2013).

16. Baumgartner, M., Bayer, F., Pfrunder-Cardozo, K. R., Buckling, A. & Hall, A. R. Resident microbial communities inhibit growth and antibiotic-resistance evolution of Escherichia coli in human gut microbiome samples. *PLoS Biol.* **18,** e3000465 (2020).

17. Eng, R., Smith, S. & Cherubin, C. Inoculum effect of new beta-lactam antibiotics on Pseudomonas aeruginosa. *Antimicrob. Agents. Chemother.* **26,** 42–47 (1984).

18. Geller, L. T., Barzily-Rokni, M., Danino, T., *et al.* Potential role of intratumor bacteria in mediating tumor resistance to the chemotherapeutic drug gemcitabine. *Science* **357,** 1156–1160 (2017).

19. Grossman, T. H. Tetracycline antibiotics and resistance. *Cold Spring Harb. Perspect. Med.* **6,** a025387 (2016).

20. Burke, K. E. & Lamont, J. T. Fecal Transplantation for Recurrent Clostridium difficile Infection in Older Adults: A Review. *J. Am. Geriatr. Soc.* **61,** 1394–1398 (2013).

21. Blair, J. M., Bavro, V. N., Ricci, V., *et al.* AcrB drug-binding pocket substitution confers clinically relevant resistance and altered substrate specificity. *Proc. Natl. Acad. Sci. U.S.A.* **112,** 3511–3516 (2015).

22. Whittle, G, Whitehead, T. R., Hamburger, N, Shoemaker, N. B., Cotta, M. A., *et al.* Identification of a new ribosomal protection type of tetracycline resistance gene, tet(36), from swine manure pits. *Appl. Environ. Microbiol.* **64,** 4151–4158 (2003).

23. Epe, B & Woolley, P. The binding of 6-demethylchlortetracycline to 70S, 50S and 30S ribosomal particles: a quantitative study by fluorescence anisotropy. *EMBO J.* **3,** 121–126 (1984).

24. Duong, M. T.-Q., Qin, Y., You, S.-H. & Min, J.-J. Bacteria-cancer interactions: bacteria-based cancer therapy. *Exp. Mol. Med.* **51,** 1–15 (2019).

25. Lawrence, D., Fiegna, F., Behrends, V., *et al.* Species interactions alter evolutionary responses to a novel environment. *PLoS Biol.* **10,** e1001330 (2012).

26. Hawley, T. S., Hawley, R. G. & Telford, W. G. Fluorescent proteins for flow cytometry. *Curr. Protoc. Cytom.* **80,** 9–12 (2017).

27. Maser, A., Peebo, K., Vilu, R. & Nahku, R. Amino acids are key substrates to Escherichia coli BW25113 for achieving high specific growth rate. *Res. Microbiol.* **171,** 185–193 (2020).

28. Cooper, V. S. The origins of specialization: insights from bacteria held 25 years in captivity. *PLoS biology* **12,** e1001790 (2014).

29. Seth, E. C. & Taga, M. E. Nutrient cross-feeding in the microbial world. *Front. Microbiol.* **5,** 350 (2014).

V. Supplementary Text

Sensitivity modulation by species S_2 is independent of resistance mechanism. In the main text, I defined whether species S_2 is sensitive to drug A based on the numerical value of κ_j in equation 3—which denotes the affinity of drug A for its target. This is equivalent to mutations, say, in the bacterial ribosome that reduce the affinity of ribosome-binding antibiotics for their target (*1*). But other resistance mechanisms such, as efflux pumps, do not act on the binding affinity of a drug for its target. Efflux pumps can have broad specificity (*2*), thus, able to protect against multiple drugs simultaneously (*3*, *4*).

To explore whether the predictions in the main text are robust to different mutation types, I redefined equations 1b and c to accommodate efflux pumps as resistance mechanism (*5*):

$$\dot{S}_j = \overbrace{G_j(C)S_j}^{\text{Growth}} \cdot \overbrace{I_j(A)}^{\text{Inhibition}}, \tag{4a}$$

$$\dot{A}_j = \overbrace{-dA_j}^{\text{Decay}} + \overbrace{\left(\varphi_j(A_e - A_j) - \frac{v^* p_j}{k_m^* + p_j}\right) S_j}^{\text{Fick's Diffusion with Efflux}}, \tag{4b}$$

$$\dot{A}_e = -dA_e - \sum_{j=1}^{i} \left(\varphi_j(A_e - A_j) - \frac{v^* p_j}{k_m^* + p_j}\right) S_j, \tag{4c}$$

$$\dot{C} = -\sum_{j=1}^{i} \overbrace{U_j(C)S_j}^{\text{C-Uptake}}, \tag{4d}$$

Here v^* represents the maximal efflux rate; k_m^* the half-saturation constant associated where the affinity of the pump for its substrate, A, is given by $1/k_m^*$; and $0 \leq p_j \leq 1$ is the expression level of $j-1$ copies of the efflux pump gene based on the limited abundance of DNA polymerase transcription complex (*6*). The abundance of this pump depends on the number of genes $j-1$ encoding efflux pump. The parameter p_j is monotonically increasing and bounded in j, controlled by a dimensionless constant γ in the Michaelis-Menten function $p_j = (j-1)/(1+\gamma(j-1))$ and $p_j/(k_m^* + p_j)$ the probability that a given drug molecule is bound to the pump. Thus, species S_1 does not express any efflux pump (no copies, as $j-1=0$) whereas species S_2 does indeed express the efflux pump. The remaining parameters are described in the main text with $\kappa_1 = \kappa_2$.

As Figure S6 illustrates, efflux pumps do not change the effect that competing genotypes have on species S_1. However, this resistance mechanism does increase even further the relative abundance of drug A in species S_1. Drug A also diffuses into competing species S_2 until it reaches equilibrium, and will diffuse back into the environment as the abundance of A declines, effectively re-exposing S_1. Active efflux exacerbates this effect by actively moving A molecules from within S_2 back into the environment. The result, shown in Figures S6A–C, is further inhibition of S_1 with respect to the mechanism used in the main text, as noted by its lower IC_{90}.

Supplementary References

1. Hu, M., Nandi, S., Davies, C. & Nicholas, R. A. High-level chromosomally mediated tetracycline resistance in Neisseria gonorrhoeae results from a point mutation in the rpsJ gene encoding ribosomal protein S10 in combination with the mtrR and penB resistance determinants. *Antimicrobial agents and chemotherapy* **49,** 4327–4334 (2005).
2. Murakami, S., Nakashima, R., Yamashita, E. & Yamaguchi, A. Crystal structure of bacterial multidrug efflux transporter AcrB. *Nature* **419,** 587–593 (2002).
3. Eckford, P. D. & Sharom, F. J. ABC efflux pump-based resistance to chemotherapy drugs. *Chem. Rev.* **109,** 2989–3011 (2009).
4. Blair, J. M., Bavro, V. N., Ricci, V., *et al.* AcrB drug-binding pocket substitution confers clinically relevant resistance and altered substrate specificity. *Proc. Natl. Acad. Sci. U.S.A.* **112,** 3511–3516 (2015).
5. Ayari, Jessica, P., Fabio, G., *et al.* Using a Sequential Regimen to Eliminate Bacteria at Sublethal Antibiotic Dosages. *PLoS Biol.* **13,** e1002104 (Apr. 2015).
6. Nierlich, D., Rutter, W. & Fox, C. *Molecular Mechanisms in the Control of Gene Expression* Fig. 3 in p.139. ISBN: 9781483273938 (Elsevier Science, 2013).

VI. Supplementary Figures

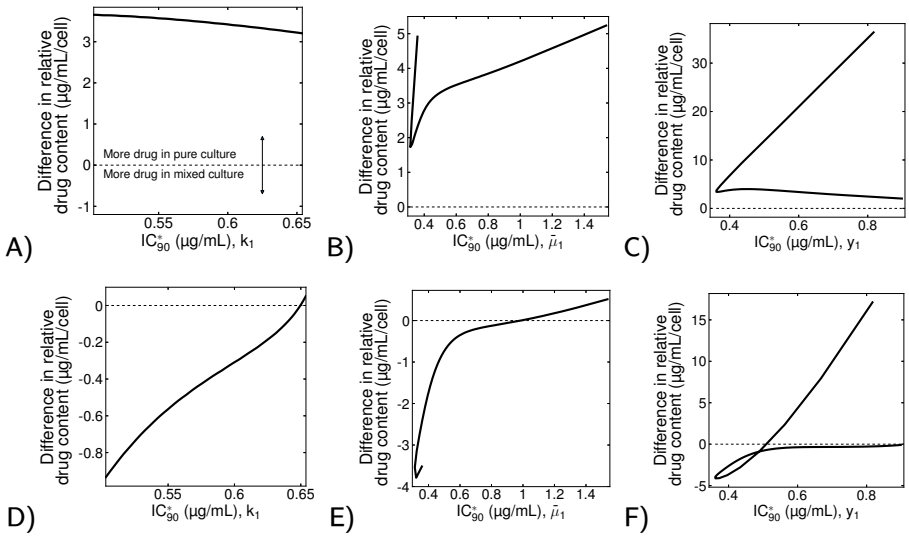

Figure S1. Difference in drug content in cells from species S_1 in pure and mixed growth conditions. A–C) Theoretical difference in relative drug content—antibiotic molecules per cell–of S_1 between pure culture conditions, and mixed culture with *drug-sensitive* S_2. A), B) and C) illustrate the prediction when changing the parameter k, $\bar{\mu}$, and y, respectively. The difference is positive (>0) when the relative content of antibiotic is higher in pure culture conditions, whereas is negative (<0) when the content is higher in mixed culture conditions. Lack of difference is represented by a horizontal, dotted line. **D–F)** Theoretical difference in relative drug content—antibiotic molecules per cell–of S_1 between pure culture conditions, and mixed culture with *drug-insensitive* S_2. A), B) and C) illustrate the prediction when changing the parameter k, $\bar{\mu}$, and y, respectively. The difference is positive (>0) when the relative content of antibiotic is higher in pure culture conditions, whereas is negative (<0) when the content is higher in mixed culture conditions. Lack of difference is represented by a horizontal, dotted line.

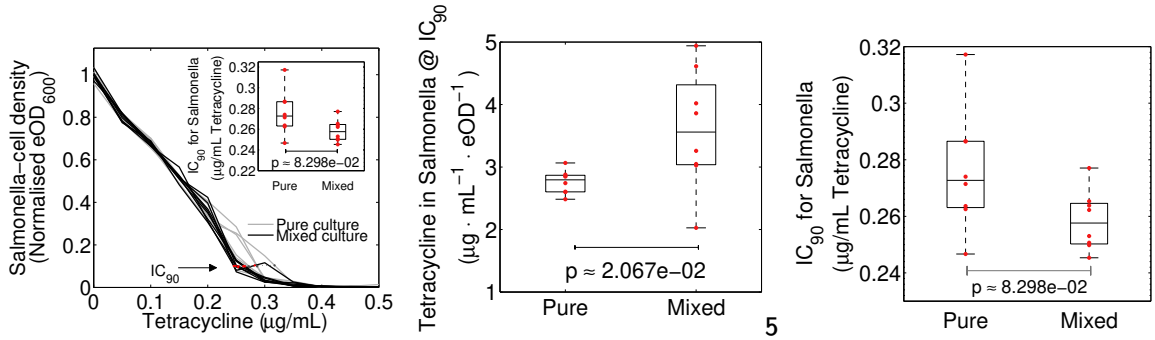

Figure S2. Drug efficacy data for *Salmonella typhimurium*. Left) Change in normalised density of *Salmonella typhimurium* as a function of tetracycline concentration, when Wyl grows in mixed culture with tetracycline-sensitive *Escherichia coli* Wyl. The change in density of *S. typhimurium* growing in mixed culture is shown in black, with grey showing the change in density in pure culture. The IC_{90} in each condition is shown as dots, red for mixed culture conditions and dark grey for pure culture, connected by a dotted line. Non-parametric, Mann-Whitney U-test between IC_{90}s is shown in the inset. Raw data is shown as dots, whereas the boxes represent median (centre of the box), 25th, and 75th percentile of the dataset. The whiskers show the most extreme data points that are not outliers. Similar box plots show the relative content of tetracycline in *S. typhimurium* at its IC_{90} (**centre**), and changes in IC_{90} berween pure and mixed culture conditions (**right**)

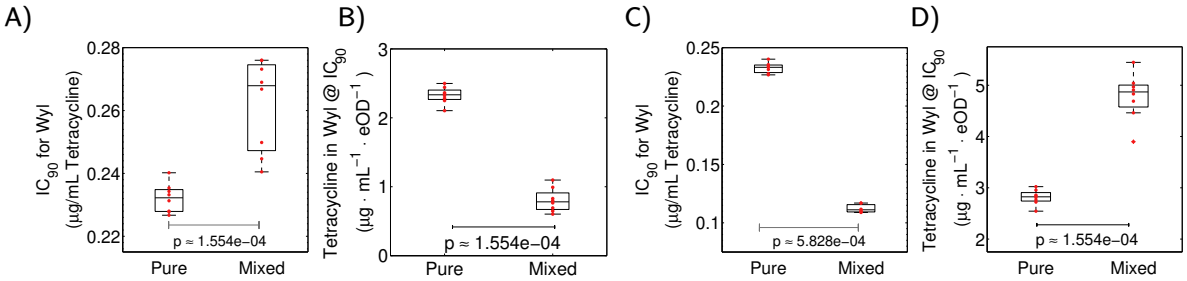

Figure S3. Box plots for tetracycline efficacy against *Escherichia coli*. The boxes represent median (centre of the box), 25th, and 75th percentile of the dataset for IC_{90} and drug content in *Escherichia coli* Wyl growing alongside drug-sensitive *Salmonella typhimurium* (A and B), and drug-resistant *Escherichia coli* GB(c). The whiskers show the most extreme data points that are not outliers. The *p* values shown correspond to non-parametric Mann-Whitney U-tests to determine significance of the difference in datasets between pure and mixed culture conditions.

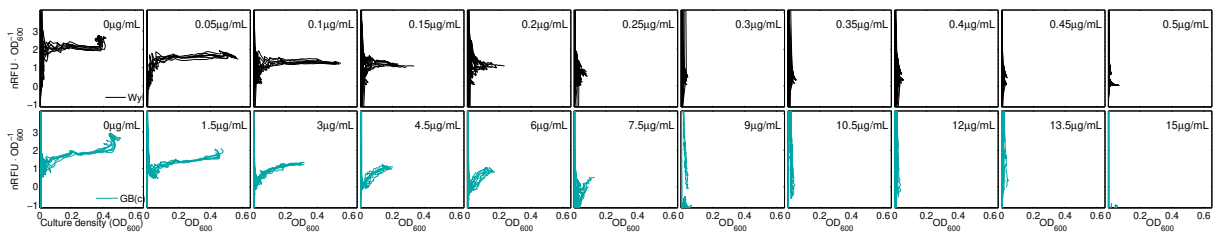

Figure S4. Changes in relative fluorescence over time in both Wyl and GB(c) strains of *Escherichia coli*. Raw change in florescence, per optical density units, measured every 20min for 24h for *E. coli* Wyl (black) and GB(c). Each column represents the data set for each tetracycline concentration used.

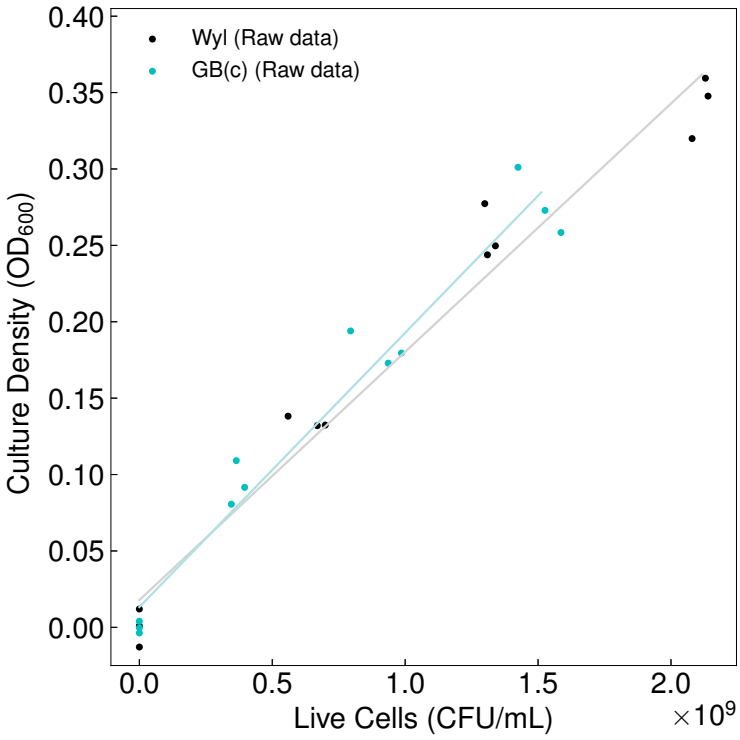

Figure S5. Calibration curve to translate optical density data to number of *Escherichia coli* cells. I fitted the linear model $a = bx + c$ to optical density and colony counting data (dots) to calculate the number of optical density units (OD_{600}) per cell. a denotes the optical density readings measured at 600nm, c the crossing point with the $y-$axis when $x = 0$, and b the conversion factor between optical density and number of cells (x). I interpolating optical density readings to calculate the number of cells within a culture as $x = (a - c)/b$. For the strain S, $b = 1.62 \times 10^{-10}\ OD \cdot mL \cdot CFU^{-1}$ and $c = 1.78 \times 10^{-2}\ OD$, whereas for R $b = 1.79 \times 10^{-10}\ OD \cdot mL \cdot CFU^{-1}$ and $c = 1.33 \times 10^{-2}\ OD$.

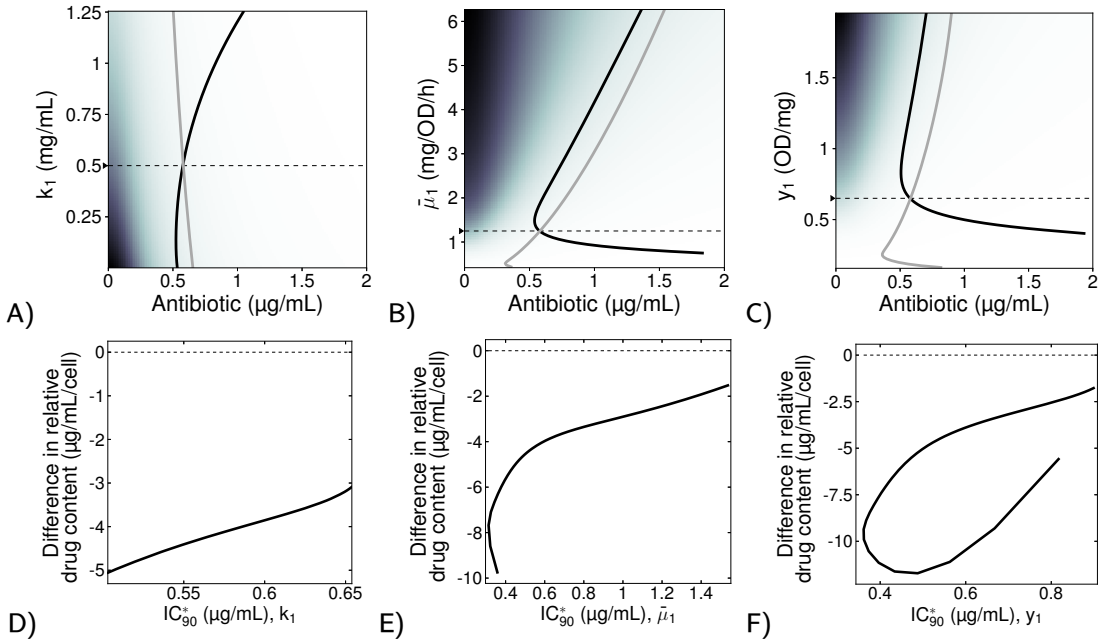

Figure S6. Drug concenttration in individuals from species S_1 in pure and mixed growth conditions when competing genotypes avoid drug-inhibition through efflux pumps. A–C) IC_{90}, antibiotic concentration inhibiting 90% (IC_{90}) the growth predicted without drug, resulting with different parameters values for the half-saturation parameter k_1 (B), maximal carbon up-take $\bar{\mu}_1$ (C), or biomass yield y_s (D) in equation 1 when species S_2 is drug-resistant through efflux pumps. The IC_{90} for species S_1 growing as pure cultures is shown in grey, and growing in mixed culture with S_2 are shown in black. The parameter values for species S_2 were fixed at a value noted by a black arrow on the y-axis, followed by a dotted black line. **D–F)** Theoretical difference in relative drug content—antibiotic molecules per cell–of S_1 between pure culture conditions, and mixed culture with *drug-insensitive* S_2. D), E) and F) illustrate the prediction when changing the parameter k, $\bar{\mu}$, and y, respectively. The difference is positive (>0) when the relative content of antibiotic is higher in pure culture conditions, whereas is negative (<0) when the content is higher in mixed culture conditions. Lack of difference is represented by a horizontal, dotted line.